Enhanced solar-light-driven photocatalysis by carbon-nanodots/nanodiamonds heterojunction

Xiaochen Sun, Chen Wang, Lu Liu, Qiliang Wang, Shaoheng Cheng, Nan Gao, Junsong Liu*, Hongdong Li

State Key Lab of Superhard Materials, College of Physics, Jilin University, Changchun 130012, China, emails: jsliu@jlu.edu.cn (J. Liu), sxc19@mails.jlu.edu.cn (X. Sun), chenw18@mails.jlu.edu.cn (C. Wang), liulu2012@126.com (L. Liu), wangqiliang@jlu.edu.cn (Q. Wang), chengshaoheng@jlu.edu.cn (S. Cheng), gaon@jlu.edu.cn (N. Gao), hdli@jlu.du.cn (H. Li)

ABSTRACT

In this study, the carbon dots/nanodiamonds (CDs/NDs) heterojunction is synthesized through microwave heating treatment with the mixed solution of citric acid, urea and NDs as precursor. The CDs/NDs show superior photocatalytic efficiency (98.1% MB degradation) and a higher rate constant (17.9×10^{-3} min^{-1}). The high photocatalytic performance of CDs/NDs materials is attributed to the enhanced separation of photogenerated carriers. This study indicates that the unique CDs/NDs heterojunction is the potential for the rapid and efficient treatment of organic pollutants in wastewater.

Keywords: Photocatalysis; Carbon nanodots; Nanodiamonds

1. Introduction

As a promising technology against environmental problems, the photocatalysis driven by solar light has attracted much attention [1]. Traditionally, semiconductor materials of TiO_2, ZnO, and Cu_2O have been widely used as photocatalysts over several decades, due to their economic nature, chemical inertness, and resistant to corrosion [2–4]. However, these semiconductor photocatalysts usually show ultraviolet range activity, due to their wide band gaps [2,5]. Moreover, it is still a significant challenge to attain efficient durable charge separation for photocatalysis with semiconductor photocatalysts [6,7]. Nowadays, the preparation of prominent photocatalyst is still core technology [8,9], and the wide photo absorption range and high separation efficiency of the photogenerated charge carriers are necessary for an ideal photocatalyst [10].

As a kind of zero-dimensional semiconductor, carbon quantum dots (CDs) are distinctive from other carbon nanomaterials, due to their unique physical, chemical, electronic, and optical properties [11,12], which make them possible applied in many fields. Especially, the CDs have been widely used to enhance the photocatalytic efficiency in recent years [13]. Actually, CDs act as a hole acceptor to promote photogenerated carrier separation, due to their excellent carrier transfer ability, it could also be used as electron reservoirs and photosensitizers in visible-light-driven photocatalysis [14–16]. It is known that the photocatalysis kinetics significantly enhanced when the surface structure of the photocatalyst is modified [13]. Hence, the heterostructures of semiconductor catalysts (such as TiO_2, ZnO, Bi_2WO_6, etc.) with CDs are found to further promote their charges separation along with transportation, and ultimately the photocatalytic activity enhances [2,17–20]. Therefore, it is interesting to exploit a novel composited semiconductor related to CDs as a heterostructure photocatalyst.

The nanodiamonds (NDs) have excellent carrier mobility and large specific surface area, facilitating the transfer of

* Corresponding author.

photogenerated carriers to the photocatalyst surface [14,21], and creating more reactive chemical surface groups [14,19], thus, the NDs have been widely used to as catalysts [22], composites [23] and magnetic sensors [24]. Nowadays, the NDs are successfully produced in large amounts at low cost and less toxic, due to the advanced and environmentally friendly purification techniques [25,26]. Furthermore, the advantages of high room temperature thermal conductivity, chemical stability, breakdown voltage, and resistance to photobleaching insure NDs against the thermal, chemical, and electric damages during the process of photocatalysis or photo-electrocatalysis [14,27]. However, the photocatalytic performance of CDs/NDs heterojunction has not been studied yet.

In this study, the preparation, characterization, photocatalytic activity, and mechanism of CDs/NDs heterojunction as a green photocatalyst are investigated.

2. Experimental section

2.1. Microwave synthesis of CDs/NDs

Microwave heating treatment was utilized to synthesize CDs/NDs composites with citric acid, urea and NDs mixed solution as precursor. First, 0.600 g of urea and 3.000 g of citric acid were dissolved into 10 mL of ultrapure water in a glass beaker. Second, 0.046 g of NDs with the average particle size of ~5 nm was dispersed adequately into the citric acid-urea solution via ultrasonic processing. Third, the mixed solution was put in a microwave oven (WD900B, GalanZ) for microwave treatment at 900 W, until the solution was evaporated to dryness and dark-brown solid was produced. Fourth, the samples were centrifuged and washed with ethanol until the pH value reached approximately 7, following the samples were dried at vacuum drying oven (DZG-6020, Senxin) to further dehydrate at 75°C for 6 h. Finally, the dry solid was grinded into powder with an agate mortar. Then, the powder of CDs/NDs composite material was obtained. In addition, CDs were prepared according to above procedures without adding NDs.

2.2. Characterization

The microstructures were indicated by a transmission electron microscopy (TEM) (JEOL JEM2100). The crystal lattice structures were shown by X-ray diffraction (XRD) (XRD-6000 Shimadzu, China Life Building, 16 Chaowai Street, Chaoyang District, Beijing) and high-resolution transmission electron microscopy (HRTEM) (JEOL JEM2100). Fourier transform infrared (FTIR) spectroscopies were conducted using the Nicolet (Thermo Fisher Building 6, 27 Xinjinqiao Road, Pudong, Shanghai) spectrometer with a resolution of 4 cm^{-1}. Photoluminescence properties were recorded by a Horiba Jobin Yvon spectrometer with an excitation wavelength of 330 nm.

2.3. Photocatalytic activity measurements

The photocatalytic activity of CDs/NDs composites was evaluated with Methylene blue (MB). A 500 W Xe lamp (GXZ500) was used as the simulated solar light source. The distance between the lamp and suspension was 15 cm.

Typically, 0.002 g of catalysts including CDs, NDs, and CDs/NDs, respectively, were dispersed in an aqueous MB solution (50 mL, 10 mg L^{-1}) and magnetically stirred in the dark for 1 h to attain the adsorption–desorption equilibrium. Next, 200 μL of H$_2$O$_2$ were added into each photoreactor, then it was illuminated under solar light. Then, at certain time intervals, 3 mL suspension was withdrawn from the reaction and subjected to centrifugation. The MB concentration was monitored using a UV-vis spectrophotometer (UV-1240 Shimadzu) at the wavelength of 664 nm.

3. Results and discussion

3.1. Characterization of CDs/NDs composites

The CDs/NDs particles with nearly uniform size are shown in TEM (Fig. 1a). The ND is coated with CDs, and granularity analysis software (Nano Measurer 1.2) shows that the mean diameter of CDs/NDs is 6.45 nm (Fig. 1b). As shown HRTEM image in Fig. 1c, the lattice fringe spacing of 0.206 nm corresponds to (111) crystal plane of diamond [28,29]. The strong diffraction spots in the selected area electron diffraction (SAED) pattern confirms the evidence of crystalline diamond. Furthermore, the rings correspond to the (111), (220), and (311) crystal planes of diamond [30]. The ratio for the square of the ring radius of 3:8:11 indicates the diamond structure. It demonstrates that the heterojunction consists of CDs and NDs.

The XRD over a range of 2θ angles from 10° to 70° is shown in Fig. 2. The broad peak centered at 23° is assigned to the amorphous carbon [31]. In the diffraction pattern of NDs, the peak at 43.9° is assigned to the (111) plane of cubic diamond [14,25]. The obvious peak at 23° and 43.9° in the XRD pattern of CDs/NDs indicates the materials is primarily composed of NDs and amorphous carbon.

FTIR spectra of CDs, NDs, and CDs/NDs are presented in Fig. 3. The peaks at 1,184; 1,384; and 1,713 cm^{-1} belong to the C–O–C symmetrical stretching vibration, C–H in-plane bending vibration, and C=O stretching vibration in COOH, respectively [2,7,13,32]. The peaks at 1,641 cm^{-1} of NDs is ascribed to C=O [33]. The broad band in the range of the 3,300–3,700 cm^{-1} are assigned to compound with hydroxyl group O–H stretching vibration, which represents the huge number of outstanding hydroxyl groups on the surface of the CDs, NDs, and CDs/NDs [7,34]. The presence of hydrophilic and carboxyl functional groups over CDs and CDs/NDs surface denotes the excellent water solubility [2,35].

To study the optical properties of CDs, NDs, and CDs/NDs, UV-vis absorption is carried out. As illustrated in Fig. 4, the absorption spectrum of CDs exhibits a broad peak around the range of 250–290 nm, which is ascribed to the typical absorption of an aromatic π system or the *n–p** transition of the carbonyl [33,36], and it is found to be broader in CDs/NDs. Two peaks at 248 and 350 nm appeared in the excitation spectrum, and the absorption peak at around 350 nm underwent a slight redshift after combining with NDs, which means the increased N-doping level. As a result, the CDs/NDs has a better external quantum yields compare with CDs [4].

As a typical signature, photoluminescence behavior is considered as most significant property for CDs [2].
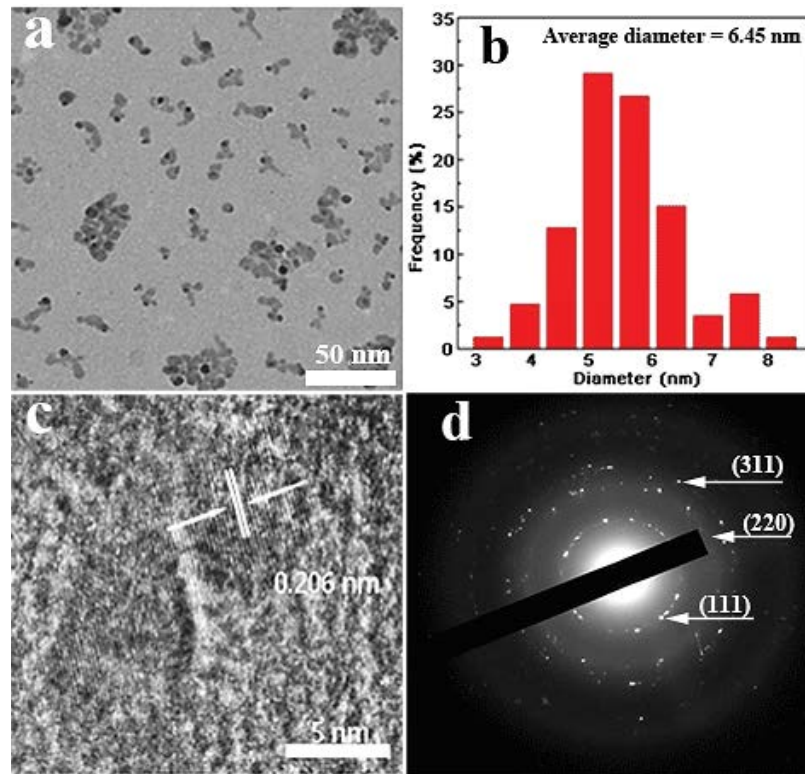
Fig. 1. TEM of (a) CDs and (b) corresponding size-distribution graph, (c) HRTEM of CDs/NDs, and (d) SAED pattern of CDs/NDs.
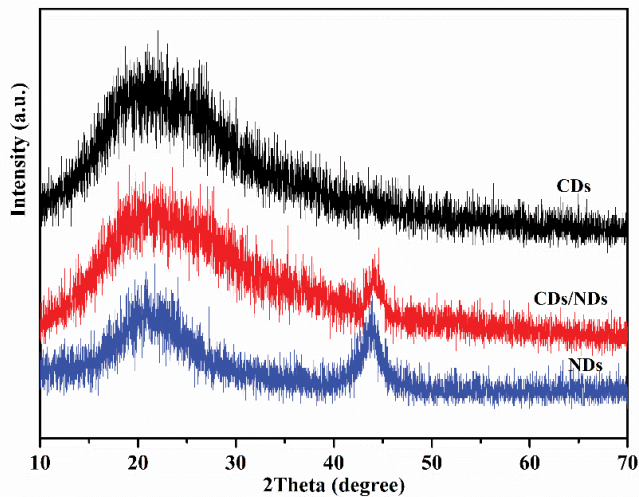
Fig. 2. XRD spectra of CDs, CDs/NDs, and NDs.

Fig. 3. FTIR spectra of CDs, CDs/NDs, and NDs.

Fluorescence emission spectra of CDs, NDs, and CDs/NDs demonstrated in Fig. 5 clearly reveal that the emission peaks of CDs and CDs/NDs locate at 428 nm. Remarkably, the emission intensity increases significantly after adding NDs, it suggests that hybridization of NDs and CDs as a novel heterojunction could highly improve the separation efficiency of photogenerated electrons and holes [7]. The band gap is determined by applying the Tauc model in the high absorbance region following the equation: $\alpha h\nu = D(h\nu - E_g)^n$, where α, h, v, D, and E_g represent the absorption coefficient,

Planck's constant, light frequency, proportionality constant and band gap, respectively [37]. Furthermore, the n value is determined by the features of the transition for a semiconductor: $n = 1/2$ for direct transition (CDs) and $n = 2$ for indirect transition (NDs) [38,39]. Therefore, combined with the tauc plots calculated from UV-vis absorbance spectra, the bandgaps of CDs and NDs are calculated to be 2.16 and 3.25 eV, respectively.
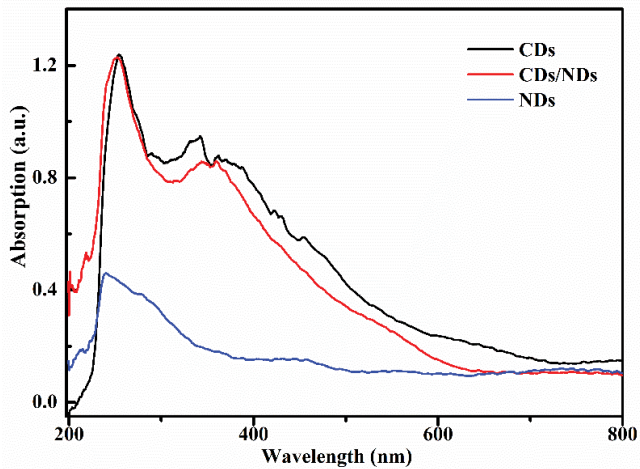
Fig. 4. UV-vis absorption spectra for CDs, NDs, and CDs/NDs.
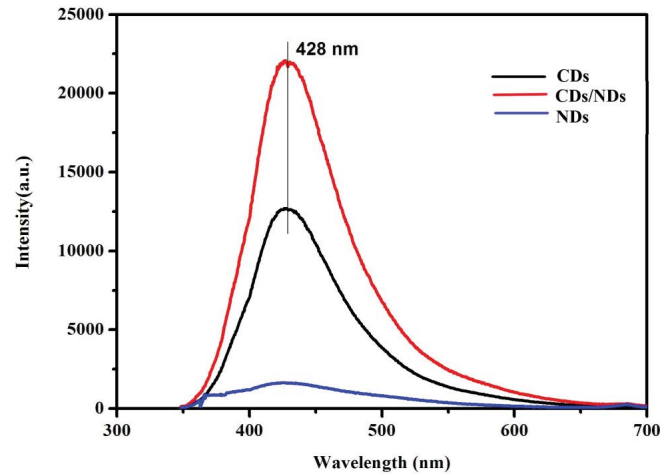
Fig. 5. Photoluminescence spectra of CDs, NDs, and CDs/NDs.

3.2. Photocatalytic degradation of MB

The degradation efficiency of the as-prepared samples is defined as follows [7,40]:

$$\text{Degradation } (\%) = \left(\frac{1-C}{C_0} \right) \times 100\% \qquad (1)$$

where C and C_0 represent the MB concentration at time t and the equilibrium, respectively. The error analysis is calculated using the following standard deviation formula [13]:

$$\sigma^2 = \lim_{n \to \infty} \left[\frac{1}{N} \Sigma \left(x_i - \mu \right)^2 \right] \qquad (2)$$

where σ is the standard deviation, x_i is the observed value, and μ is the mean value.

As shown in Fig. 6a, 64.9% MB is removed with bare H_2O_2 at the solar-light irradiation time of 210 min. After the solar-light irradiation for 210 min, 98.1% of MB is photodegraded by CDs/NDs, while only 88.9% (66.1%) of MB is degraded by bare CDs (NDs) with equal amount of H_2O_2. The results denote that CDs/NDs exhibit better photocatalytic performance than bare CDs and NQs for MB degradation.

Moreover, the kinetics of MB degradation is investigated in Fig. 6b. The experimental data are fitted with the pseudo-first-order-kinetic equation by Eq. (3) [7,13]:

$$\ln\left(\frac{C}{C_0} \right) = -kt \qquad (3)$$

where k is the apparent reaction rate constant (min^{-1}). The values of k are obtained by non-linear regression, and the results are shown in Table 1, where it is clearly shown that the apparent rate constant of CDs/NDs (17.9 × 10^{-3} min^{-1}) for MB degradation is obviously higher than CDs and NDs (10.1 × 10^{-3} and 5.8 × 10^{-3} min^{-1}). It denotes that the composite materials of NDs and CDs can enhance the photocatalytic activity to degrade MB with H_2O_2.
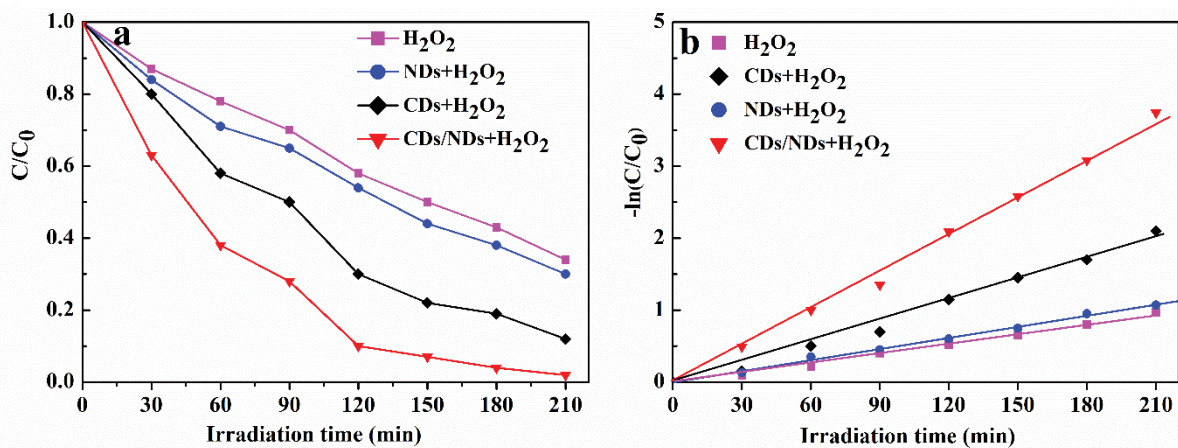
Fig. 6. (a) Photocatalytic degradation of MB in the presence of H_2O_2, CDs + H_2O_2, NDs + H_2O_2, and CDs/NDs + H_2O_2 under solar-light irradiation (error bars represent standard deviation of triplicate runs) and (b) kinetic fit for the degradation of MB.

Table 1
Pseudo-first-order rate constants (k) of MB degradation when using H_2O_2, CDs + H_2O_2, NDs + H_2O_2, and CDs/NDs + H_2O_2 as photocatalytic reagents

Photocatalytic reagents	k (10^{-3} min^{-1})
H_2O_2	4.9
CDs + H_2O_2	10.1
NDs + H_2O_2	5.8
CDs/NDs + H_2O_2	17.9

3.3. Photocatalytic mechanism of CDs/NDs

As a strong oxidizing agent, HO$^\bullet$ radical generated by the decomposition of H_2O_2 under solar-light irradiation could decolorize most of MB dye as follows [13,41]:

$$H_2O_2 + h\nu \rightarrow 2HO \tag{4}$$

$$MB\ (C_{16}H_{18}ClN_3S, 3H_2O) + HO^\bullet \rightarrow Degradation \tag{5}$$

Therefore, 65% MB is removed with bare H_2O_2 at the solar-light irradiation time of 210 min (Fig. 6).

The CDs could produce electron-hole pairs under solar-light irradiation [16]. Furthermore, CDs exhibit excellent optical property of down- and up-converted photoluminescence, and the ability to absorb long wavelength light and producing radicals with solution species, which makes CDs widely used in photocatalysis [42]. To illustrate the electronic structures of CDs, molecular orbital (MO) theory is widely used [43]. In most cases, $n \rightarrow \pi^*$ and $\pi \rightarrow \pi^*$ transitions could easily occur in CDs, due to their low transition energies [44]. The π-states can be ascribed to aromatic sp^2-hybridized carbons, which could form π-MO through the overlap of vertical P_Z orbital [44]. Because of the $\pi–\pi$ conjugation effect in CDs, the energy gap between π-states and π^*-states decreases gradually, as the number of conjoint aromatic rings increases [43,45]. The n-states of CDs could be ascribed to functional groups containing electron lone pairs in heteroatoms. If the heteroatoms with electron lone pairs are bonded to aromatic sp^2-hybridized carbons, electron transitions can occur from the n-states of the heteroatoms to the π^*-states of the aromatic rings ($n \rightarrow \pi^*$) [44].

When CDs is used to enhance the photocatalytic effects on MB degradation with H_2O_2 under solar-light irradiation, the ground states of CDs can be excited into excited states, due to the electron transitions from nonbonding orbital and π bonding orbital to π antibonding orbital ($n \rightarrow \pi^*$ and $\pi \rightarrow \pi^*$). Then, the photoinduced electrons could produce superoxide radical anions $O_2^{\bullet-}$ and H_2O_2 through scavenging the molecular oxygen, which adsorbs on the CDs surface [13,46].

$$CDs + h\nu\ (solar\ light) \rightarrow CDs\ (e_{cb}^- + h_{vb}^+) \tag{6}$$

$$O_2 + e_{cb}^- \rightarrow O_2^{\bullet-} \tag{7}$$

$$2H^+ + O_2 + 2e^- \rightarrow H_2O_2 \tag{8}$$
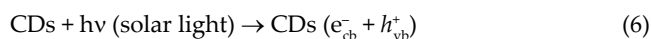
The photogenerated hole (h_{vb}^+) can oxidize OH$^-$ or H_2O into OH radical [13,46]:

$$H_2O + h_{vb}^+ \rightarrow HO^\bullet + H^+ \tag{9}$$

$$H_2O_2 + O_2^{\bullet-} \rightarrow HO^\bullet + O_2 + OH^- \tag{10}$$

$$MB\ (C_{16}H_{18}ClN_3S, 3H_2O) + h_{vb}^+ \rightarrow Oxidation \tag{11}$$

$$MB\ (C_{16}H_{18}ClN_3S, 3H_2O) + e_{cb}^- \rightarrow Reduction \tag{12}$$

$$MB\ (C_{16}H_{18}ClN_3S, 3H_2O) + HO^\bullet \rightarrow Degradation \tag{13}$$
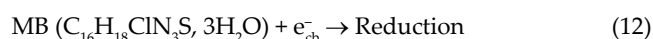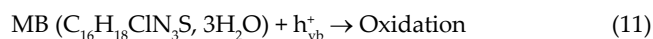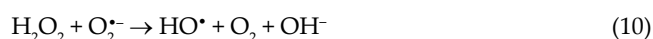
The as-produced superoxide radical anions ($O_2^{\bullet-}$) and hole produced by the transfer of photoinduced electron would oxidize the MB dye as follows [13,47]:

$$MB\ (C_{16}H_{18}ClN_3S, 3H_2O) + O_2^{\bullet-} \rightarrow CO_2 + H_2O \tag{14}$$

$$MB\ (C_{16}H_{18}ClN_3S, 3H_2O) + h_{vb}^+ \rightarrow CO_2 + H_2O \tag{15}$$
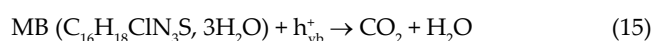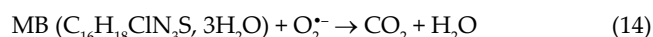
In addition, the H_2O_2 molecules adsorbed on CDs could be decomposed into HO$^\bullet$ radicals with strong oxidation ability, which efficiently oxidizes the MB [1,42]. Therefore, the semiconductor photocatalytic mechanism is one of pathways for CDs to photodegrade MB.

The effect of dye sensitization on MB photodegradation under visible light irradiation should not be neglected. Excited MB is able to inject an electron into the conduction band of CDs. Usually, the photocatalysis of MB with CDs under visible light irradiation involves the following reactions [41]:

$$MB + h\nu\ (visible\ light) \rightarrow MB^* \tag{16}$$

$$MB^\bullet + CDs \rightarrow MB^{\bullet+} + CDs\ (e^-) \tag{17}$$

$$CDs\ (e^-) + O_2 \rightarrow CDs + O_2^{\bullet-} \tag{18}$$

$$MB^{\bullet+} \rightarrow degradation\ of\ MB^{\bullet+} \tag{19}$$
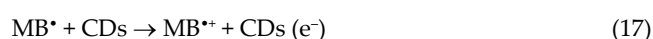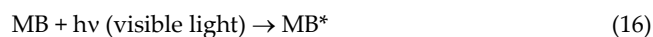
After losing an electron, the MB molecule (i.e., D$^{\bullet+}$) could react with hydroxyl ions to produce HO$^\bullet$ radicals, which can oxidize MB efficiently via steps (20) and (21), or interact with other radical species (i.e., $O_2^{\bullet-}$, HOO$^\bullet$, or HO$^\bullet$) to generate intermediates those ultimately lead to CO_2 [41].

$$MB^{\bullet+} + OH^- \rightarrow MB + HO \tag{20}$$

$$MB + 2HO^\bullet \rightarrow H_2O + oxidation\ products \tag{21}$$

$$O_2^{\bullet-} + H^+ \rightarrow HOO \tag{22}$$

$$HOO^\bullet + H^+ + CDs\ (e^-) \rightarrow H_2O_2 + CDs \tag{23}$$

$$H_2O_2 + CDs\ (e^-) \rightarrow HO^\bullet + OH^- + CDs \tag{24}$$

$$MB^{\bullet+} + O_2^{\bullet-} \rightarrow DO_2 \rightarrow products \tag{25}$$

$$MB^{\bullet+} + HOO^\bullet\ (or\ HO^\bullet) \rightarrow products \tag{26}$$
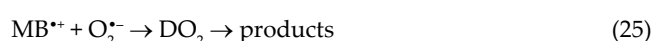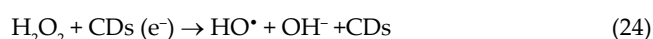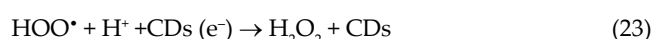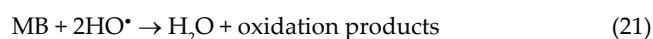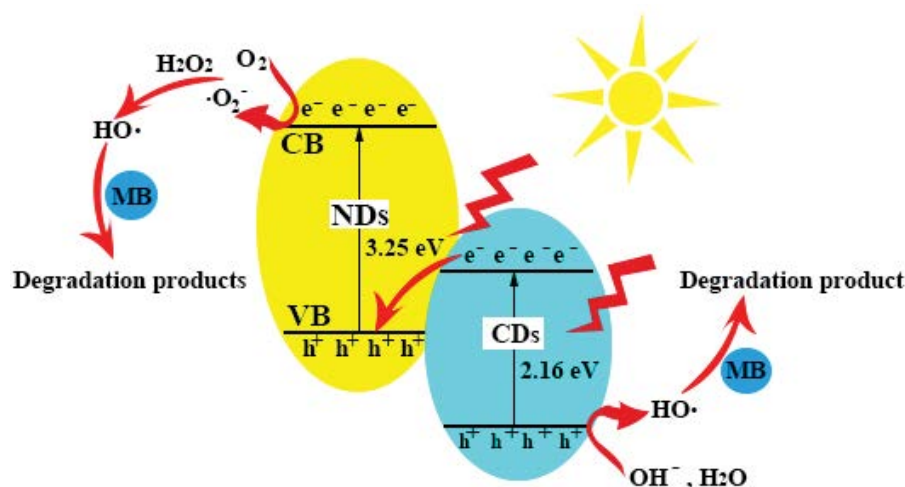
Fig. 7. Proposed mechanism of solar-light-driven photodegradation of MB with CDs/NDs photocatalyst and H_2O_2.

Therefore, dye sensitization is another pathway for CDs to photodegrade MB.

It has been reported that the bound π electron in sp^2-hybridized C atoms is weak, and free electrons will produce, when the π orbitals overlap effectively [14,48]. In this situation, the electronic coupling between NDs and CDs occurs, which would influence the electronic structures of NDs and CDs. In CDs/NDs, because of the suitable band structure between CDs and NDs, including staggered bands, large Fermi level difference, and the electron-donating behavior of CDs, photogenerated carriers at the CDs/NDs interface cannot recombine [14,42,49]. Furthermore, NDs has been considered a promising photocatalyst materials owing to its high carrier mobility, large specific surface area, small Bohr radius and large exciton binding energy, which may quickly capture the photogenerated carriers in the adjacent CDs and promote carrier separation [14]. The enhanced mechanism of the solar-light-driven photodegradation of MB with the CDs/NDs demonstrated in Fig. 7. The band gaps of CDs and NDs are determined to be 2.16 and 3.25 eV from the Tauc plot of UV-vis absorption spectra, the corresponding valence band maximum (VBM) and conduction band minimum (CBM) are 2.35 and –0.9 eV for NDs [39,50] and 3.57 and 1.41 eV for CDs, respectively. Therefore, the hole in the VBM of NDs prefers to recombine with the electron from the electron-rich CBM of CDs [51], to form the direct *Z*-scheme heterojunction photocatalyst. Thus, the separation of the photogenerated charges is facilitated, decreasing the occurrence of electron-hole recombination and leading to an increase of the CDs/NDs photocatalytic activity.

4. Conclusions

The CDs/NDs heterojunction is synthesized through a facile microwave method. The photocatalytic activities of CDs/NDs are evaluated by the photodegradation of MB, which is used as the target organic pollutant. After the hybridization with NDs, the photocatalytic activity of CDs for the degradation of MB increases dramatically under solar-light irradiation. CDs/NDs display superior photocatalytic efficiency with nearly 98.1% removal of MB (10 mg/L) in 210 min, while only 88.9% of MB is degraded by bare CDs. Moreover, the apparent rate constant of CDs/NDs (17.9×10^{-3} min^{-1}) for MB degradation is also higher than CDs (10.1×10^{-3} min^{-1}). The excellent photocatalytic performance of CDs/NDs materials is attributed to the enhanced separation of photogenerated carriers.

References

[1] K.Q. Lu, Q. Quan, N. Zhang, Y.J. Xu, Multifarious roles of carbon quantum dots in heterogeneous photocatalysis, J. Energy Chem., 25 (2016) 927–935.
[2] A. Tyagi, K.M. Tripathi, N. Singh, S. Choudhary, R.K. Gupta, Green synthesis of carbon quantum dots from lemon peel waste: applications in sensing and photocatalysis, RSC. Adv., 6 (2016) 72423–72432.
[3] T. Pandiyarajan, R. Saravanan, B. Karthikeyan, F. Gracia, H.D. Mansilla, M.A. Gracia-Pinilla, R.V. Mangalaraja, Sonochemical synthesis of CuO nanostructures and their morphology dependent optical and visible light driven photocatalytic properties, J. Mater. Sci. - Mater. Electron., 28 (2017) 2448–2457.
[4] R. Shi, Z. Li, L.Z. Wu, H.J. Yu, L. Shang, Effect of nitrogen doping level on the performance of N-doped carbon quantum dot/TiO$_2$ composites for photocatalytic hydrogen evolution, ChemSusChem, 10 (2017) 4650–4656.
[5] M.N. Chong, J.B. Chow, C. Saint, Recent developments in photocatalytic water treatment technology: a review, Water Res., 44 (2010) 2997–3027.
[6] W. Wang, Y.R. Ni, Z.Z. Xu, One-step uniformly hybrid carbon quantum dots with high-reactive TiO$_2$ for photocatalytic application, J. Alloys Compd., 622 (2015) 303–308.
[7] A.J. Cai, Q. Wang, Y.F. Chang, X.P. Wang, Graphitic carbon nitride decorated with S,N co-doped graphene quantum dots for enhanced visible-light-driven photocatalysis, J. Alloys Compd., 692 (2017) 183–189.
[8] K. Antil-Martini, D. Contreras, J. Yanez, L. Cornejo, P. Santander, H.D. Mansilla, Solar light driven oxidation of gentisic acid on ZnO, Sol. Energy, 142 (2017) 26–32.

[9] K. Natarajan, H.C. Bajaj, R.J. Tayade, Direct sunlight driven photocatalytic activity of GeO$_2$/monoclinic-BiVO$_4$ nanoplate composites, Sol. Energy, 148 (2017) 87–97.

[10] H.J. Yu, R. Shi, Y.F. Zhao, I.N. Geoffrey, L.Z. Wu, C.H. Tung, T. Zhang, Smart utilization of carbon dots in semiconductor photocatalysis, Adv. Mater., 28 (2016) 9454–9477.

[11] S.N. Baker, G.N. Baker, Luminescent carbon nanodots: emergent nanolights, Angew. Chem. Int. Ed., 49 (2010) 6726–6744.

[12] S. Sharma, V. Dutta, P. Singh, P. Raizada, A.R. Sani, A.H. Bandegharaei, V.K. Thakur, Carbon quantum dot supported semiconductor photocatalysts for efficient degradation of organic pollutants in water: a review, J. Cleaner Prod., 228 (2019) 755–769.

[13] V. Ramar, S. Moothattu, K. Balasubramanian, Metal free, sunlight and white light based photocatalysis using carbon quantum dots from *Citrus grandis*: a green way to remove pollution, Sol. Energy, 169 (2018) 120–127.

[14] Z.Y. Lin, J. Xiao, L.H. Li, P. Liu, C.X. Wang, G.W. Yang, Nanodiamond-embedded p-type copper(I) oxide nanocrystals for broad-spectrum photocatalytic hydrogen evolution, Adv. Energy Mater., 6 (2016) 1501865, doi: 10.1002/aenm.201670027.

[15] H.T. Li, X.Y. Zhang, D.R. MacFarlane, Carbon quantum dots/Cu$_2$O heterostructures for solar-light-driven conversion of CO$_2$ to methanol, Adv. Energy Mater., 5 (2015) 1401077, doi: 10.1002/aenm.201401077.

[16] M. Han, S.J. Zhu, S.Y. Lu, Y.B. Song, T.L. Feng, S.Y. Tao, J.J. Liu, B. Yang, Recent progress on the photocatalysis of carbon dots: classification, mechanism and applications, Nano Today, 19 (2018) 201–218.

[17] H.J. Yu, Y.F. Zhao, C. Zhou, L. Shang, Y. Peng, Y.H. Cao, L.Z. Wu, C.H. Tung, T.R. Zhang, Carbon quantum dots/TiO$_2$ composites for efficient photocatalytic hydrogen evolution, J. Mater. Chem. A, 2 (2014) 3344–3351.

[18] A. Prasannan, T. Imae, One-pot synthesis of fluorescent carbon dots from orange waste peels, Ind. Eng. Chem. Res., 52 (2013) 15673–15678.

[19] F. Li, F. Tian, C.J. Liu, Z. Wang, Z.J. Du, R.X. Li, L. Zhang, One-step synthesis of nanohybrid carbon dots and TiO$_2$ composites with enhanced ultraviolet light active photocatalysis, RSC Adv., 5 (2015) 8389–8396.

[20] R. Atchudan, T.N.J.I. Edison, S. Perumal, R. Vinodh, Y.R. Lee, *In-situ* green synthesis of nitrogen-doped carbon dots for bioimaging and TiO$_2$ nanoparticles@nitrogen-doped carbon composite for photocatalytic degradation of organic pollutants, J. Alloys Compd., 766 (2018) 12–24.

[21] M. Baidakova, A. Vul', New prospects and frontiers of nanodiamond clusters, J. Phys. D: Appl. Phys., 40 (2007) 6300–6311.

[22] J.A. Zhang, D.S. Su, R. Blume, R. Schlogl, R. Wang, X.G. Yang, A. Gajovic, Surface chemistry and catalytic reactivity of a nanodiamond in the steam-free dehydrogenation of ethylbenzene, Angew. Chem. Int. Ed., 49 (2010) 8640–8644.

[23] V.N. Mochalin, I. Neitzel, B.J.M. Etzold, A. Peterson, G. Palmese, Y. Gogotsi, Covalent incorporation of aminated nanodiamond into an epoxy polymer network, ACS Nano, 5 (2011) 7494–7502.

[24] J.R. Maze, P.L. Stanwix, J.S. Hodges, S. Hong, J.M. Taylor, P. Cappellaro, L. Jiang, M.V.G. Dutt, E. Togan, A.S. Zibrov, A. Yacoby, R.L. Walsworth, M.D. Lukin, Nanoscale magnetic sensing with an individual electronic spin in diamond, Nature, 455 (2008) 644–647.

[25] M.J. Sampaio, L.M. Pastrana-Martinez, A.M.T. Silva, J.G. Buijnsters, C. Han, C.G. Silva, S.A.C. Carabineiro, D.D. Dionysiou, J.L. Faria, Nanodiamond-TiO$_2$ composites for photocatalytic degradation of microcystin-LA in aqueous solutions under simulated solar light, RSC Adv., 5 (2015) 58363–58370.

[26] V.N. Mochalin, O. Shenderova, D. Ho, Y. Gogotsi, The properties and applications of nanodiamonds, Nat. Nanotechnol., 7 (2012) 11–23.

[27] Y.C. Lin, K.J. Sankaran, Y.C. Chen, C.V. Lee, H.C. Chen, I.N. Lin, N.H. Tai, Enhancing electron field emission properties of UNCD films through nitrogen incorporation at high substrate temperature, Diamond Relat. Mater., 20 (2011) 191–195.

[28] Z.J. Qiao, J.J. Li, N.Q. Zhao, C.S. Shi, P. Nash, Graphitization and microstructure transformation of nanodiamond to onion-like carbon, Scr. Mater., 54 (2006) 225–229.

[29] V.L. Kuznetsov, I.L. Zilberberg, Y.V. Butenko, A.L. Chuvilin, B. Segall, Theoretical study of the formation of closed curved graphite-like structures during annealing of diamond surface, J. Appl. Phys., 86 (1999) 863–870.

[30] S.R.J. Pearce, S.J. Henley, F. Claeyssens, P.W. May, K.R. Hallam, J.A. Smith, K.N. Rosser, Production of nanocrystalline diamond by laser ablation at the solid/liquid interface, Diamond Relat. Mater., 13 (2004) 661–665.

[31] S.Q. Wang, N.Q. Zhao, C.S. Shi, E. Liu, C. He, F. He, L.Y. Ma, *In-situ* grown CNTs modified SiO$_2$/C composites as anode with improved cycling stability and rate capability for lithium storage, Appl. Surf. Sci., 433 (2018) 428–436.

[32] Q.H. Liang, W.J. Ma, Y. Shi, Z. Li, X.M. Yang, Easy synthesis of highly fluorescent carbon quantum dots from gelatin and their luminescent properties and applications, Carbon, 60 (2013) 421–428.

[33] M. Zheng, H. Ming, H. Huang, Y. Liu, Z.H. Kang, One-step ultrasonic synthesis of fluorescent N-doped carbon dots from glucose and their visible-light sensitive photocatalytic ability, New J. Chem., 36 (2012) 861–864.

[34] L. Shi, L. Liang, J. Ma, F.X. Wang, J.M. Sun, Remarkably enhanced photocatalytic activity of ordered mesoporous carbon/g-C$_3$N$_4$ composite photocatalysts under visible light dagger, Dalton Trans., 43 (2014) 7236–7244.

[35] H. Peng, J. Travas-Sejdic, Simple aqueous solution route to luminescent carbogenic dots from carbohydrates, Chem. Mater., 21 (2009) 5563–5565.

[36] P.C. Hsu, H.T. Chang, Synthesis of high-quality carbon nanodots from hydrophilic compounds: role of functional groups, Chem. Commun., 48 (2012) 3984–3986.

[37] H.F. Yin, Y. Cao, T. Fan, B. Qiu, M. Zhang, J. Yao, P.F. Li, X.H. Liu, S. Chen, Construction of carbon bridged TiO$_2$/CdS tandem Z-scheme heterojunctions toward efficient photocatalytic antibiotic degradation and Cr(VI) reduction, J. Alloy Compd., 824 (2020) 153915, doi: 10.1016/j.jallcom.2020.153915.

[38] X. Yang, H. Li, Y. Li, X. Lv, G. Zou, Synthesis and optical properties of purified translucent, orthorhombic boron nitride films, J. Cryst. Growth, 312 (2010) 3434–3437.

[39] L.X. Su, Q.Z. Huang, Q. Lou, Z.Y. Liu, J.L. Sun, Z.T. Zhang, S.R. Qin, X. Li, J.H. Zang, L. Dong, C.X. Shan, Effective light scattering and charge separation in nanodiamond@g-C$_3$N$_4$ for enhanced visible-light hydrogen evolution, Carbon, 139 (2018) 164–171.

[40] Z.A.C. Ramli, N. Asim, W.N.R.W. Isahak, Z. Emdadi, N. Ahmad-Ludin, M.A. Yarmo, K. Sopian, Photocatalytic degradation of methylene blue under UV light irradiation on prepared carbonaceous TiO$_2$, Sci. World J., 8 (2014) 415136, doi: 10.1155/2014/415136.

[41] C. Galindo, P. Jacques, A. Kalt, Photodegradation of the aminoazobenzene acid orange 52 by three advanced oxidation processes: UV/H$_2$O$_2$, UV/TiO$_2$ and VIS/TiO$_2$ - comparative mechanistic and kinetic investigations, J. Photochem. Photobiol., A, 130 (2000) 35–47.

[42] Z.J. Zhang, T.T. Zheng, X.M. Li, J.Y. Xu, H.B. Zeng, Progress of carbon quantum dots in photocatalysis applications, Part. Part. Syst. Char., 33 (2016) 457–472.

[43] H.T. Li, X.D. He, Z.H. Kang, H. Huang, Y. Liu, J.L. Liu, S.Y. Lian, C.H.A. Tsang, X.B. Yang, S.T. Lee, Water-soluble fluorescent carbon quantum dots and photocatalyst design, Angew. Chem. Int. Ed., 49 (2010) 4430–4434.

[44] R. Wang, K.Q. Lu, Z.R. Tang, Y.J. Xu, Recent progress in carbon quantum dots: synthesis, properties and applications in photocatalysis, J. Mater. Chem. A, 5 (2017) 3717–3734.

[45] R.L. Smith, R.Q. Zhang, Infinite horizon production planning in time-varying systems with convex production and inventory costs, Manage. Sci., 44 (1998) 1313–1320.

[46] I.K. Konstantinou, T.A. Albanis, TiO$_2$-assisted photocatalytic degradation of azo dyes in aqueous solution: kinetic and mechanistic investigations - a review, Appl. Catal., B, 49 (2004) 1–14.

[47] A. Sharma, M. Varshney, J. Park, T.K. Ha, K.H. Chae, H.J. Shin, XANES, EXAFS and photocatalytic investigations on copper oxide nanoparticles and nanocomposites, RSC Adv., 5 (2015) 21762–21771.

[48] K.V. Reich, E.D. Eidelman, Effect of electron-phonon interaction on field emission from carbon nanostructures, Europhys. Lett., 85 (2009) 47007, doi: 10.1209/0295-5075/85/47007.

[49] Z.Y. Lin, P. Liu, J.H. Yan, G.W. Yang, Matching energy levels between TiO_2 and alpha-Fe_2O_3 in a core-shell nanoparticle for visible-light photocatalysis, J. Mater. Chem. A, 3 (2015) 14853–14863.

[50] D.D. Sang, H.D. Li, S.H. Cheng, Q.L. Wang, Q. Yu, Y.Z. Yang, Electrical transport behavior of n-ZnO nanorods/p-diamond heterojunction device at higher temperatures, J. Appl. Phys., 112 (2012) 036101, doi: 10.1063/1.4745039.

[51] J.X. Low, C.J. Jiang, B. Cheng, S. Wageh, A. Al-Ghamdi, J. Yu, A review of direct Z-scheme photocatalysts, Small Methods, 1 (2017) 1700080, doi: 10.1002/smtd.201700080.